

Self-similar non-equilibrium dynamics of a many-body system with power-law interactions

Ricardo Gutiérrez, Juan P. Garrahan, and Igor Lesanovsky

School of Physics and Astronomy, University of Nottingham, Nottingham, NG7 2RD, UK

(Dated: September 3, 2022)

The influence of power-law interactions on the dynamics of many-body systems far from equilibrium is much less explored than their effect on static and thermodynamic properties. To gain insight into this problem we introduce and analyze here an out-of-equilibrium deposition process in which the deposition rate of a given particle depends as a power-law on the distance to previously deposited particles. Although rather simplistic this model draws its relevance from recent experimental progress in the domain of cold atomic gases which are studied in a setting where atoms that are excited to high-lying Rydberg states interact through power-law potentials that translate into power-law excitation rates. The out-of-equilibrium dynamics of this system turns out to be surprisingly rich. It features a self-similar evolution which leads to a characteristic power-law time dependence of observables such as the particle concentration and results in a scale invariance of the structure factor. Moreover, it displays a crossover to a mean-field regime as a function of the power-law exponent. Our findings show that in dissipative Rydberg gases out of equilibrium the characteristic distance among excitations — often referred to as the blockade radius — is not a static but rather a dynamic quantity.

PACS numbers: 67.85.-d, 05.30.-d, 32.80.Ee, 05.65.+b

Self-similar behaviour is ubiquitous in physics. It emerges for example in condensed matter systems near criticality [1], in biological systems [2] as well as in complex networks [3]. Systems with this property “look the same” under a rescaling of characteristic length and/or time scales. This property often entails a drastic reduction of the details that are necessary for a theoretical description, such as specific parameter values or initial conditions. Self-similar behaviour can also occur in cold atomic ensembles, currently used as an experimental platform for exploring fundamental questions of far-from-equilibrium physics such as the approach of interacting many-body systems to (thermal) equilibrium [4–6]. For example, self-similar behavior is predicted for the relaxation of a gas of quenched Bose-condensed atoms as a consequence of the existence of non-thermal fixed points [7, 8]. Moreover, it is argued [9] that many of these characteristics were also present during the evolution of the early universe leading to the idea of using cold atomic systems as analogue systems for addressing problems of relevance to cosmology or particle physics.

In this work we introduce a simple far-from-equilibrium scenario in which a non-trivial relaxation dynamics is driven by power-law interactions. The motivation stems from recent experiments in the domain of cold atom physics which explore the laser excitation of atoms to high-lying electronic states in which they interact with power-law potentials. While complementary, the scenario we study below has analogies with that of the above-mentioned work on Bose-condensed gases [7–9]. In particular, evolution which is initially fast and uncorrelated is succeeded by slow and strongly correlated self-similar growth. We show that the physics of this dynamics is governed by an effective particle deposition

process where the rates depend on the distance to other deposited particles as a power-law. The scale-invariant nature of the deposition dynamics is revealed analytically and confirmed numerically by means of extensive numerical simulations. Moreover, we show that the relaxation dynamics crosses over into a mean-field regime when the power-law exponent becomes equal to the system dimension. Beyond providing an understanding of non-equilibrium processes governed by power-law interactions our results reveal new insights into the relaxation behaviour of gases of interacting Rydberg atoms, which are currently widely employed for the experimental study of many-body phenomena [10–16]. Our results indicate that the characteristic minimal distance between Rydberg excitations — which is often referred to as blockade radius — is not generally a static quantity but can in the presence of dissipation acquire a non-trivial scale-invariant time-dependence. Finally, we illuminate the impact of genuine long-range interactions (i.e. power-law interactions with exponent equal to or smaller than the dimensions of the embedding space) on the non-equilibrium dynamics.

The dynamical problem we study below emerges from considering a collection of N atoms on a cubic lattice in d dimensions. Each atom is described with two levels, a ground state and the excited Rydberg state, denoted as $|\downarrow\rangle$ and $|\uparrow\rangle$ respectively. Atoms in the Rydberg state at positions \mathbf{r}_k and \mathbf{r}_m interact through a power-law potential $V_{km}^{(\alpha)} = C_\alpha/|\mathbf{r}_k - \mathbf{r}_m|^\alpha$ with exponent α , while the much weaker interactions involving atoms in the ground state are neglected. Typically encountered exponents are $\alpha = 6$ (van der Waals interaction) and $\alpha = 3$ (dipolar interaction) [17]. The atomic states $|\uparrow\rangle$ and $|\downarrow\rangle$ are resonantly coupled by a laser field and at the same time

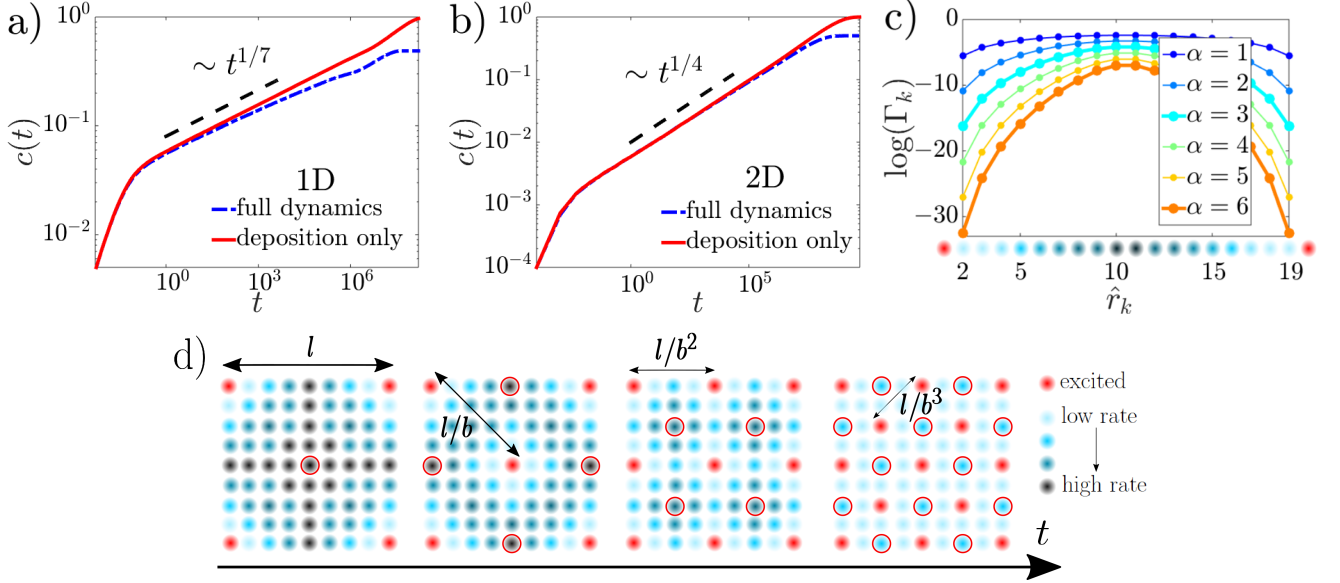


FIG. 1. **Deposition process vs. full Rydberg gas dynamics.** (a) Concentration $c(t)$ of excitations as a function of time in a 1D chain of $N = 10^4$ atoms interacting through a power-law potential ($\alpha = 3$, $R = 15$) for the full process (deposition and removal; blue dashed line) and for pure deposition (red continuous line). The dot-dashed segment corresponds to a power-law with exponent $d/(2\alpha + d) = 1/7$. See text for details. (b) Same results for a $N = 100 \times 100$ 2D square lattice. The dot-dashed segment corresponds to a power-law of exponent $1/4$. (c) Deposition rate Γ_k [Eq. (1)] as a function of \hat{r}_k in a 1D lattice ($R = 15$) with excitations being present on sites 1 and 20. (The most relevant cases, $\alpha = 3$ and 6, are accentuated.) (d) Sketch of the deposition model in a 2D lattice. Red (blue) discs represent excited (ground state) atoms. The darker the blue the higher the deposition rate for subsequent excitations. Encircled discs indicate the most likely positions for deposition.

subject to strong dissipation which leads to the rapid dephasing of superposition states, e.g. $|\uparrow\rangle + |\downarrow\rangle$. The evolution of the system is governed by a (classical) spin-flip dynamics in which a change in the state of site k , whether an excitation $|\downarrow\rangle \rightarrow |\uparrow\rangle$ or a de-excitation $|\uparrow\rangle \rightarrow |\downarrow\rangle$, occurs with an (operator-valued) rate (see Ref. [18])

$$\Gamma_k^{-1} = 1 + \left[R^\alpha \sum_{m \neq k} \frac{n_m}{|\hat{\mathbf{r}}_k - \hat{\mathbf{r}}_m|^\alpha} \right]^2. \quad (1)$$

Here R [19] parameterizes the interaction strength, $n_k = |\uparrow\rangle_k \langle \uparrow|$ is the excitation number operator and $\hat{\mathbf{r}}_k = \mathbf{r}_k/a$ are position vectors in units of the lattice constant a . The term $R^\alpha \sum_{m \neq k} n_m / |\hat{\mathbf{r}}_k - \hat{\mathbf{r}}_m|^\alpha$ strongly correlates the atoms, giving rise to a slowing down of the dynamics in the vicinity (within a distance R) of an excited atom. In this sense, the dynamics is affected by kinetic constraints of the type that are usually considered in simplified models of the glass transition [20]. This description of the Rydberg gas dynamics has been recently used in a number of theoretical works [18, 21–26] and was also successfully employed to model experiments [12, 16].

We consider an 'empty' initial state, $|\mathcal{C}(0)\rangle = |\downarrow\downarrow\downarrow\cdots\downarrow\rangle$. One key observation that greatly helps to simplify the following analysis is that excitation processes $|\downarrow\rangle \rightarrow |\uparrow\rangle$ strongly dominate over de-excitations $|\uparrow\rangle \rightarrow |\downarrow\rangle$. Thus, the effective reversible dynamics is in essence a pure (and

irreversible) *deposition process* (where $|\uparrow\rangle \rightarrow |\downarrow\rangle$ is not allowed) governed by the following master equation

$$\partial_t |P(t)\rangle = \sum_k \Gamma_k [\sigma_+^k - (1 - n_k)] |P(t)\rangle. \quad (2)$$

The vector $|P(t)\rangle \equiv \sum_{\mathcal{C}} P(\mathcal{C}; t) |\mathcal{C}\rangle$, with $P(\mathcal{C}; t)$ denoting the probability of finding a specific configuration of excitations $|\mathcal{C}\rangle$ at time t . The operator σ_+^k creates an excitation at site k , or — in the deposition picture — deposits a particle in site k . Figure 1 shows the concentration of excitations $c(t) \equiv \sum_k \langle n_k(t) \rangle / N$ as a function of time for the case of $\alpha = 3$. We see from Figs. 1(a) and 1(b) [1D chain and a 2D square lattice, respectively] that irreversible deposition processes indeed dominate the growth regime, similar to what was suggested recently in Ref. [27]. Deviations become apparent in the long-time limit when the system approaches its stationary state: for the reversible process this is the fully random state, $\lim_{t \rightarrow \infty} c(t) = 1/2$, while for the deposition process it is the (absorbing) state of a full lattice, $\lim_{t \rightarrow \infty} c(t) = 1$. Note, that in the case of Rydberg gases this long-time limit will typically not be achieved due to the finite lifetime of excited atoms. However, the initial phases of the growth dynamics are well within the reach of current experiments.

In the strongly correlated regime, i.e. when the inter-particle distance becomes smaller than R , the deposition process is amenable to an approximate analytical treat-

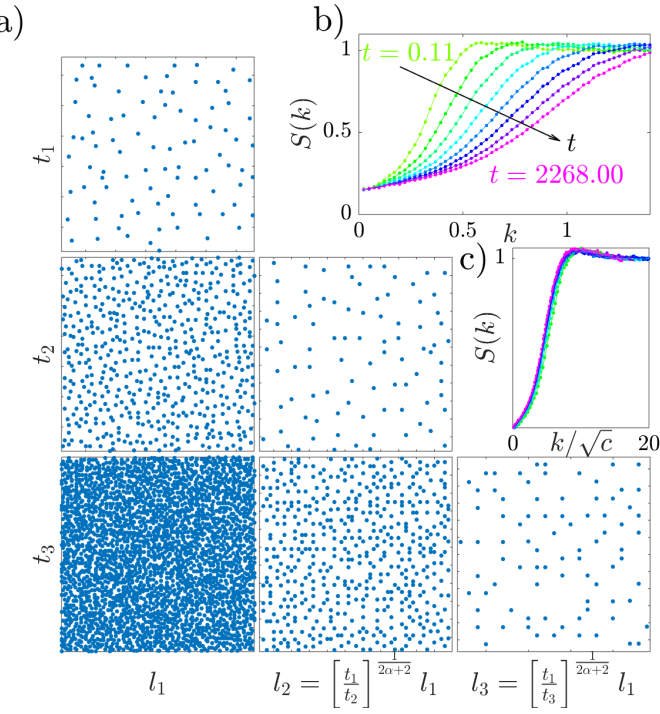


FIG. 2. **Scale invariant evolution.** (a) Excitations (blue dots) in a 2D square lattice of $N = 256 \times 256$ atoms, $\alpha = 3$ and $R = 15$. The first column shows a subsystem of size $l_1 \times l_1$ sites for $l_1 = 128$ system at three different times: $t_1 = 1$, $t_2 = 10^3$, $t_3 = 10^6$. The second column shows the configuration within a box of linear size $l_2 = (t_1/t_2)^{1/(2\alpha+2)}l_1 \simeq 54$ at times t_2 and t_3 . The third column shows the configuration within a box of linear size $l_3 = (t_1/t_3)^{1/(2\alpha+2)} \simeq 23$ at time t_3 . (b) Snapshots of the structure factor $S(k)$ taken at different times. (c) $S(k)$ as a function of the scaled wavenumber $k/\sqrt{c(t)}$. All the lines shown in panel (b) collapse onto a master curve.

ment. This is most transparently explained in 1D: Consider two excitations in a 1D chain separated by distance l . Then the next excitation will be deposited with very high likelihood at (essentially) a distance $l/2$ from the two existing excitations, effectively rescaling the inter-excitation distance by the factor $b = 2$. The reason for this is that the deposition rate is highly peaked at the mid point between two excitations as shown in Fig. 1(c). The process continues until the natural cutoff scale — the lattice spacing a — is reached, which makes further subdivision impossible. A similar process is expected to occur in 2D, where the same reasoning, starting for example from a square of excitations, can be applied with a rescaling constant $b = \sqrt{2}$ [see Fig. 1(d)]. That the actual dynamics indeed follows a rescaling behavior is nicely observed in Fig. 2(a) (details further below).

For a more quantitative answer we consider the distribution $\pi(l, t)$ of distances l between nearest excitations. Formalizing the above considerations suggests that its evolution is approximately described by the equation $\partial_t \pi(l, t) = N^{-1}[(bl)^d \Gamma(bl) \pi(bl, t) - l^d \Gamma(l) \pi(l, t)]$, where

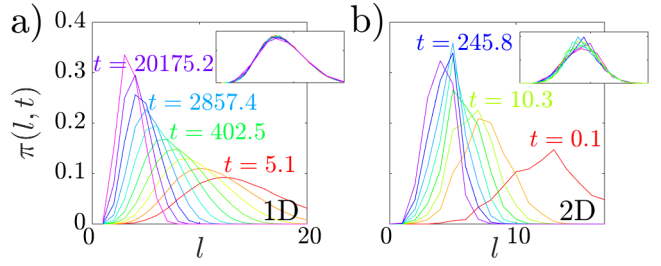


FIG. 3. **Scale invariance of $\pi(l, t)$ in 1D and 2D.** (a) Distribution of distances between nearest excitations $\pi(l, t)$ and rescaling according to Eq. 4 for $\alpha = 3$ in a 1D chain ($N = 2^{16}$, $R = 15$). Lines of different colour correspond to different times. The inset shows the collapse of the distribution functions under Eq. 4 [distributions are shown as a function of $l t^{1/(2\alpha+d)}$ and multiplied by $t^{1/(2\alpha+d)}$]. (b) Same as panel (a) for 2D ($N = 256 \times 256$, $R = 15$).

$d \leq 3$ is the dimension, $b = 2/\sqrt{d}$ is the scaling parameter and $\Gamma(l)$ is the rate at which the rescaling step $l \rightarrow l/b$ occurs. Taking the continuum limit in l we find,

$$\frac{\partial_\tau \bar{\pi}(l, \tau)}{(l/L)^{(2\alpha+d)}} = \sum_{p=1}^{\infty} \frac{(-1)^{p+1}}{p!} [(\log(b) l' \partial_{l'})^p \bar{\pi}(l', \tau)]_{l'=bl}, \quad (3)$$

where $\bar{\pi}(l, \tau) \equiv l^{(2\alpha+d)} \pi(l, \tau)$, $L = N^{1/d}$ and τ is a rescaled time. This equation has a wave-like solution of the form $\pi(l, \tau) = l^{-(2\alpha+d)} F(\tau - l^{-(2\alpha+d)})$, where $F(\cdot)$ is an undetermined function in principle dependent on the initial conditions. The details of this calculation can be found in the Supplemental Material (SM) [28].

The average distance between nearest excitations as a function of time, $\langle l(t) \rangle = \int dl l \pi(l, t) / \int dl \pi(l, t)$, can be explicitly computed for sufficiently long times and it yields $\langle l(t) \rangle \sim t^{-\frac{1}{2\alpha+d}}$ or, equivalently, $c(t) = \langle l(t) \rangle^{-d} \sim t^{\frac{d}{2\alpha+d}}$ [28]. This result justifies the use of the exponents 1/7 and 1/4 in Fig 1(a,b), which were already found by a more restrictive approximation in Ref. [18] and without the understanding of the dynamics at the level of the full distribution $\pi(l, t)$.

We can rewrite $\pi(l, t)$ (see SM [28]) as a scale invariant function for long times

$$\pi(l, t) \approx l^{-(2\alpha+d)} \bar{F}(t l^{2\alpha+d}) \quad (4)$$

which physically means that the system looks the same at any time, only the characteristic distances become shorter and shorter. The prediction of self-similarity from the approximate description in terms of $\pi(l, t)$ appears robust for the actual deposition problem, as seen from Monte-Carlo simulations of Eq. (2): Fig. 2(a) shows that the configurations of a 2D system at different times, and thus very different concentration, look statistically similar if lengths are scaled according to Eq. (4). The data in Figs. 2 (b,c) confirm this observation through the collapse of the structure factors at different times.

Furthermore, the precise scaling relation in Eq. (4) is also verified in the simulations. The numerically obtained distributions of distances between nearest excitations are shown in Fig. 3. The insets show the rescaled distributions, which nicely collapse onto a master curve. This works quite well even for small values of l , where the discreteness of the lattice introduces some roughness in the curves, especially in 2D [Fig. 3 (b)].

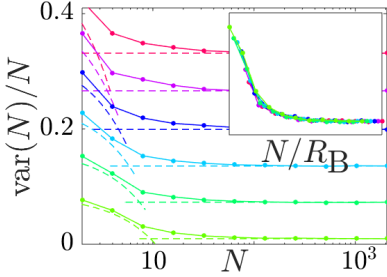


FIG. 4. **Excitation number variance as a function of the system size.** Variance in a chain of 2^{16} atoms ($\alpha = 3$, $R = 15$) for (sub-)system sizes $N = 2, 4, \dots, 2^{11}$ (averaged over 1000 realizations). The dashed curves correspond to the expression in Eq. (5) applied to each c , where R_B is extracted from the largest N considered. Different lines correspond to concentrations starting from approximately $c = 0.09$ (light green line at the bottom) to $c = 0.30$ (pink line on top) [lines have been displaced vertically to improve the visibility]. *Inset:* Number variance curves normalized by $Nc(1-c)\{1-(2R_B-1)c\}$ and plotted as functions of N/R_B .

The form of the rates (1) leads to pronounced spatial anti-correlations, i.e. there exists a “correlation hole” between excitations, cf. Figs. 1(d) and 2(a). In the context of Rydberg gases the linear size of this correlation hole is often referred to as the blockade radius R_B . Since the concentration increases in time R_B will become a dynamic quantity and thus we encounter a *dynamic Rydberg blockade*. The time-dependence of R_B can actually be inferred from a macroscopic measurement, namely the analysis of the system-size dependence of the fluctuations in the number of excitations: $\text{var}(N) = N[c(1-c) + \sum_{k \neq 0} \langle \delta n_i \delta n_{i+k} \rangle]$, where $\delta n_i \equiv n_i - c$ (with $c = \langle n_i \rangle$). Using a hard-objects description [29–32], i.e. assuming that there are no two excitations within a radius R_B , we find [28]

$$\text{var}(N) = \begin{cases} Nc(1-c)\{1-(N-1)c\}, & N \leq 2R_B \\ Nc(1-c)\{1-(2R_B-1)c\}, & N > 2R_B. \end{cases} \quad (5)$$

The left hand side is calculated numerically (or it is measured in an experiment) which allows us to extract the value of R_B . In Fig. 4 we show $\text{var}(N)$ for different times together with the approximation (5). The data collapses upon rescaling the system size by $R_B \propto t^{-\frac{1}{2\alpha+d}}$.

Finally, we consider the dependence of the deposition dynamics on the power-law exponent α . Qualitatively

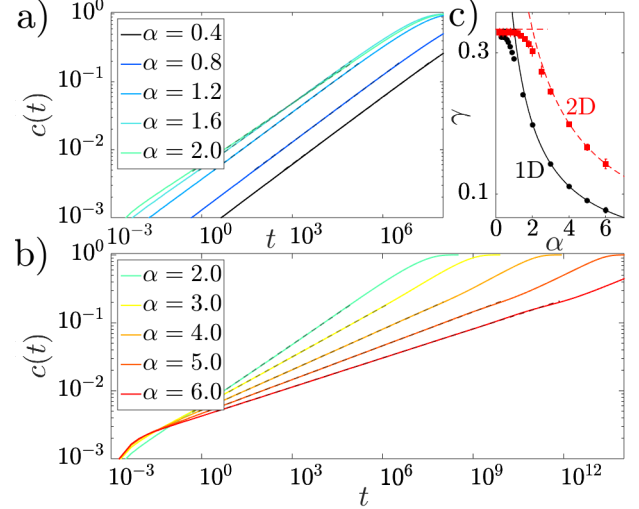


FIG. 5. **Time-evolution of the concentration for different power-law exponents α .** (a) Concentration $c(t)$ in a square lattice ($N = 317 \times 317$, $R = 15$) with long-range interactions, $\alpha \leq d = 2$ (averages of 30 realizations). The dashed segments superimposed to each line show the result of a power-law fit $c(t) \sim t^\gamma$. (b) Same as in (a) for $\alpha \geq d$. (c) Growth exponent γ vs. interaction exponent α in the same 2D square lattice (red squares) and a 1D chain (black dots; $N = 10^5$, $R = 15$). Dashed lines correspond to $\gamma = 1/3$ (mean-field exponent, for $\alpha < d$) and $\gamma = d/(2\alpha + d)$ (valid for $\alpha > d$).

there are two different situations, that of short-range interactions ($\alpha > d$) and that of long-range interactions ($\alpha \leq d$) [33]. Figure 5 shows the time evolution of the concentration in both cases. For the case where the power-law rates are short-ranged we see that the growth is exponential for very short times, and then follows the scaling law $c(t) = t^{d/(2\alpha+d)}$, cf. Eq. (4). In contrast, in the long-ranged case the concentration grows in an α -independent manner, $c(t) \sim t^\gamma$, with $\gamma \approx 1/3$ throughout (or, more precisely, after an extremely short exponential growth whose duration decreases with growing system size). The behaviour of the concentration for $\alpha \leq d$ can be understood by applying a mean-field approximation to Eq. (2) (see SM [28]).

The presented out-of-equilibrium setting is probably one of simplest manifestations of a non-trivial many-body evolution governed by power-law rates. In view of the experimental realization through Rydberg atoms it is interesting to ask how much of the observed features actually persist in the quantum regime, i.e. when the strong noise condition, which is implied by the rate equation dynamics, is lifted. While computationally unfeasible this could very well be systematically explored in the most recent generation of experiments, e.g. [10, 14, 34] and would certainly reveal interesting insights into correlated many-body dynamics.

Acknowledgements.— The research leading to these results has received funding from the European Research

Council under the European Union's Seventh Framework Programme (FP/2007-2013) / ERC Grant Agreement No. 335266 (ESCQUMA), the EU-FET grant HAIRS 612862 and from the University of Nottingham. Further funding was received through the H2020-FETPROACT-2014 grant No. 640378 (RYSQ). We also acknowledge financial support from EPSRC Grant no. EP/J009776/1. Our work has benefited from the computational resources and assistance provided by the University of Nottingham High Performance Computing service.

[1] P. M. Chaikin and T. C. Lubensky, *Principles of condensed matter physics* (Cambridge University Press, 2000); S. Sachdev, *Quantum phase transitions* (Wiley Online Library, 2007).

[2] J. H. Brown and G. B. West, *Scaling in biology* (Oxford University Press, 2000).

[3] W. E. Leland, M. S. Taqqu, W. Willinger, and D. V. Wilson, Networking, IEEE/ACM Transactions on **2**, 1 (1994); K. Park and W. Willinger, *Self-similar network traffic and performance evaluation* (Wiley Online Library, 2000); C. Song, S. Havlin, and H. A. Makse, Nature **433**, 392 (2005).

[4] T. Kinoshita, T. Wenger, and D. S. Weiss, Nature **440**, 900 (2006).

[5] S. Trotzky, Y.-A. Chen, A. Flesch, I. P. McCulloch, U. Schollwöck, J. Eisert, and I. Bloch, Nat. Phys. **8**, 325 (2012).

[6] T. Langen, S. Erne, R. Geiger, B. Rauer, T. Schweigler, M. Kuhnert, W. Rohringer, I. E. Mazets, T. Gasenzer, and J. Schmiedmayer, Science **348**, 207 (2015).

[7] J. Berges, A. Rothkopf, and J. Schmidt, Phys. Rev. Lett. **101**, 041603 (2008).

[8] A. P. Orioli, K. Boguslavski, and J. Berges, arXiv preprint arXiv:1503.02498 (2015).

[9] J. Schmiedmayer and J. Berges, Science **341**, 1188 (2013).

[10] P. Schauß, M. Cheneau, M. Endres, T. Fukuhara, S. Hild, A. Omran, T. Pohl, C. Gross, S. Kuhr, and I. Bloch, Nature **491**, 87 (2012).

[11] C. Carr, R. Ritter, C. Wade, C. Adams, and K. Weathersill, Phys. Rev. Lett. **111**, 113901 (2013).

[12] H. Schempp, G. Günter, M. Robert-de Saint-Vincent, C. Hofmann, D. Breyel, A. Komnik, D. Schölebe, M. Gärttner, J. Evers, S. Whitlock, and M. Weidemüller, Phys. Rev. Lett. **112**, 013002 (2014).

[13] N. Malossi, M. Valado, S. Scotto, P. Huillery, P. Pillet, D. Ciampini, E. Arimondo, and O. Morsch, Phys. Rev. Lett. **113**, 023006 (2014).

[14] D. Barredo, H. Labuhn, S. Ravets, T. Lahaye, A. Browaeys, and C. S. Adams, Phys. Rev. Lett. **114**, 113002 (2015).

[15] T. Weber, M. Höning, T. Niederprüm, T. Manthey, O. Thomas, V. Guarnera, M. Fleischhauer, G. Barontini, and H. Ott, Nat. Phys. **11**, 157 (2015).

[16] A. Urvoy, F. Ripka, I. Lesanovsky, D. Booth, J. Shaffer, T. Pfau, and R. Löw, Phys. Rev. Lett. **114**, 203002 (2015).

[17] M. Saffman, T. Walker, and K. Mølmer, Rev. Mod. Phys. **82**, 2313 (2010).

[18] I. Lesanovsky and J. P. Garrahan, Phys. Rev. Lett. **111**, 215305 (2013).

[19] The relation between R and the parameters in the microscopic description of the system in term of the quantum master equation is given in [18].

[20] F. Ritort and P. Sollich, Adv. Phys. **52**, 219 (2003); D. Chandler and J. P. Garrahan, Annu. Rev. Phys. Chem. **61**, 191 (2010).

[21] M. Gärttner, K. P. Heeg, T. Gasenzer, and J. Evers, Phys. Rev. A **86**, 033422 (2012).

[22] D. Petrosyan, M. Höning, and M. Fleischhauer, Phys. Rev. A **87**, 053414 (2013).

[23] D. Petrosyan, Phys. Rev. A **88**, 043431 (2013).

[24] I. Lesanovsky and J. P. Garrahan, Phys. Rev. A **90**, 011603 (2014).

[25] M. Marcuzzi, J. Schick, B. Olmos, and I. Lesanovsky, J. Phys. A **47**, 482001 (2014).

[26] M. Hoenig, W. Abdussalam, M. Fleischhauer, and T. Pohl, Phys. Rev. A **90**, 021603 (2014).

[27] J. Sanders, M. Jonckheere, and S. Kokkelmans, arXiv preprint arXiv:1504.02624 (2015).

[28] See Supplemental Material at [URL will be inserted by publisher] for detailed calculations of the self-similar solution of the deposition model, the dependence of the fluctuations on the system size and the mean-field approach to the deposition process.

[29] B. Sun and F. Robicheaux, New J. Phys. **10**, 045032 (2008).

[30] H. Weimer, R. Löw, T. Pfau, and H. P. Büchler, Phys. Rev. Lett. **101**, 250601 (2008).

[31] C. Ates and I. Lesanovsky, Phys. Rev. A **86**, 013408 (2012).

[32] M. Höning, D. Muth, D. Petrosyan, and M. Fleischhauer, Phys. Rev. A **87**, 023401 (2013).

[33] A. Campa, T. Dauxois, D. Fanelli, and S. Ruffo, *Physics of long-range interacting systems* (Oxford University Press, 2014).

[34] K. Maller, M. Lichtman, T. Xia, Y. Sun, M. Piotrowicz, A. Carr, L. Isenhower, and M. Saffman, arXiv preprint arXiv:1506.06416 (2015).

Self-similar non-equilibrium dynamics of a many-body system with power-law interactions: Supplemental Material

ANALYTICAL TREATMENT OF THE DEPOSITION MODEL

Solution of the deposition master equation in terms of $\pi(l, t)$

The dynamics of the deposition model in d -dimensions ($d = 1, 2$ or 3) is governed by the following master equation

$$\partial_t \pi(l, t) = \frac{(bl)^d}{N} \Gamma(bl) \pi(bl, t) - \frac{l^d}{N} \Gamma(l) \pi(l, t) \quad (\text{S1})$$

where $\pi(l, t)$ is the probability distribution of the distance between nearest excitations l at time t . The rate for the deposition step $l \rightarrow l/b$ is $\Gamma(l) \approx z^{-2} R^{-2\alpha} l^{2\alpha} \phi(b)$ as soon as there are excitations within distances shorter than R , according to Eq. (1) in the main text. Here, z is the coordination number of the lattice ($z = 2d$ as we consider d -dimensional cubic lattices) and $\phi(b)$ is a geometric factor that depends on the space dimensionality. For instance, in 1D $\phi(b) = [\sum_{m=0}^{N/2-1} (1/b + m)^{-1}]^{-2\alpha}$, where different terms in the sum correspond to different ‘‘shells’’ of excitations. We can therefore rewrite Eq. (S1) as

$$\partial_\tau \pi(l, \tau) = \left(\frac{bl}{L} \right)^{(2\alpha+d)} \pi(bl, \tau) - \left(\frac{l}{L} \right)^{(2\alpha+d)} \pi(l, \tau) \quad (\text{S2})$$

where $L = N^{1/d}$ is the linear size of the lattice. In order to simplify the equation, we have absorbed the factor $z^{-2} R^{-2\alpha} \phi(b) L^{2\alpha}$, which is fixed for a given lattice and interaction potential, into a rescaled time τ . The fact that $\phi(b)$ does not play any role in the derivation of the self-similar behaviour we report means that the initial condition shown in Figure 1(d) in the main text is simply a conveniently simple example for the purpose of illustration. As the normalized inter-excitation distances l/L follow $1 \rightarrow 1/b \rightarrow 1/b^2 \rightarrow \dots$, we can rewrite Eq. (S2) in terms of $\pi_n(\tau)$, the probability of having an inter-excitation distance $l = b^{-n} L$ for $n = 0, 1, 2, \dots$,

$$\partial_\tau \pi_n(\tau) = b^{-(n-1)(2\alpha+d)} \pi_{n-1}(\tau) - b^{-n(2\alpha+d)} \pi_n(\tau), \quad (\text{S3})$$

where the rhs can be most economically expressed in terms of $f_n(\tau) \equiv b^{-n(2\alpha+d)} \pi_n(\tau)$ as $f_{n-1}(\tau) - f_n(\tau)$.

What we have in Equation (S3) is the master equation in terms $\pi(l, t)$ when the deposition is such that l takes on a discrete set of values. Nevertheless, in general the initial condition $\pi(l, 0)$ is not a delta function, but a random configuration that arises from the initial creation of independent, distant excitations. Moreover, the fact that sometimes excitations do not occur exactly at the maximum of the rates forces us to consider continuous distributions where the rescaling process with parameter b takes place simultaneously at slightly different scales. To address these issues, we move on to the continuum, $l = b^{-x} L$ for $x \geq 0$, and Taylor expand $f(x, t)$ (assuming analyticity with respect to x): $f(x-1, \tau) - f(x, \tau) = -\sum_{p=1}^{\infty} \frac{1}{p!} \frac{\partial^p}{\partial x^p} f(x', t) \Big|_{x'=x-1}$. In this setting, we can rewrite the master equation back in terms of l using the function $\bar{\pi}(l, \tau) \equiv (l/L)^{(2\alpha+d)} \pi(l, \tau)$

$$(l/L)^{-(2\alpha+d)} \partial_\tau \bar{\pi}(l, \tau) = \sum_{p=1}^{\infty} \frac{(-1)^{p+1}}{p!} [(\log(b) l' \partial_{l'})^p \bar{\pi}(l', \tau)]_{l'=bl}. \quad (\text{S4})$$

Plugging in the wave-like ansatz $\bar{\pi}(l, t) = F(\tau - g(l))$ (we expect the distribution to shift towards shorter and shorter distances as time goes by), we obtain $(l/L)^{-(2\alpha+d)} F^{(1)}(\tau - g(l)) = -\log(b)(1 + \log(b)/2) F^{(1)}(\tau - g(bl))(bl) g^{(1)}(bl) - [(\log(b))^2/2] F^{(2)}(\tau - g(bl)) [(bl) g^{(1)}(bl)]^2 - [(\log(b))^2/2] F^{(1)}(\tau - g(bl))(bl)^2 g^{(2)}(bl) + \dots$, stopping at order $p = 2$. For higher orders on the rhs one obtains more terms that are (up to some constant factor, including functions of b) products of $F(\cdot)$ or its derivatives $F^{(m)}(\cdot)$ and $(bl)^m g^{(m)}(bl)$ raised to a certain power, where $g^{(m)}(bl)$ is the m -th derivative of $g(\cdot)$ evaluated at bl . As the l dependence has to cancel on both sides for the equation to hold for all times, we are left with $g(l) = l^{-(2\alpha+d)}$, and therefore (after absorbing L into the undetermined function $F(\cdot)$)

$$\pi(l, \tau) = l^{-(2\alpha+d)} F(\tau - l^{-(2\alpha+d)}). \quad (\text{S5})$$

Evolution of $c(t)$ and self-similar dynamics for long times

The mean inter-excitation distance as a function of time, $\langle l(\tau) \rangle = \int dl l \pi(l, \tau) / \int dl \pi(l, \tau)$, is, after changing the integration variables to $y = \tau - l^{-(2\alpha+d)}$,

$$\langle l(\tau) \rangle = \tau^{-\frac{1}{2\alpha+d}} \frac{\int dy (1-y/\tau)^{-\frac{2}{2\alpha+d}} F(y)}{\int dy (1-y/\tau)^{-\frac{1}{2\alpha+d}} F(y)}. \quad (\text{S6})$$

For any dilute initial condition, $F(\cdot)$ is non-zero for small values of y . On the other hand, the process spans several orders of magnitude in time (see Figure 1(a, b) in the main text), so for sufficiently long times there has to be a strong cancellation in the argument of F , and essentially $l^{-(2\alpha+d)}$ grows in parallel with τ . This means that eventually $(1-y/\tau) \approx 1$ and, writing back in terms of the original time units, $\langle l(t) \rangle \sim t^{-\frac{1}{2\alpha+d}}$, or, equivalently,

$$c(t) = l^{-d} \sim t^{\frac{d}{2\alpha+d}}. \quad (\text{S7})$$

This result is in agreement with the prediction obtained and verified in Ref. [1] by a more restrictive reasoning that did not consider the time dependence of the full distribution $\pi(l, t)$. Eq. (S7) justifies the use of the exponents 1/7 and 1/4 in Fig. 1(a, b) in the main text. By the same reasoning we can rewrite $\pi(l, t)$ as given in Eq. (S5) as a scale invariant function for long times:

$$\pi(l, t) \approx l^{-(2\alpha+d)} \bar{F}(tl^{(2\alpha+d)}), \quad (\text{S8})$$

showing that the full distribution of distances to nearest excitations evolves in a self-similar way.

So far we have considered that $\pi(l, t)$ is not normalized. If we go back to Eq. (S5) and further impose the normalization condition $C(\tau) \int dl \pi(l, \tau) = 1$ ($C(\tau)$ is a time-dependent normalization constant), through the change of variables used in Eq. (S6), we obtain

$$\frac{\tau^{-\frac{1}{2\alpha+d}}}{2\alpha+d} \int dy (1-y/\tau)^{-\frac{1}{2\alpha+d}} F(y) = C(\tau)^{-1} \quad (\text{S9})$$

which for long times indicates that a normalized $\pi(l, t)$ has to be multiplied by $C(t) \propto t^{\frac{1}{2\alpha+d}}$. Taken together, Eqs. (S8) and (S9) justify the operations performed on the numerically obtained $\pi(l, t)$ that lead to the collapse shown in Figure 3 of the main text (see the caption for an explanation).

SYSTEM-SIZE DEPENDENCE OF FLUCTUATIONS AND THE DYNAMIC BLOCKADE RADIUS

The excitation number variance at a given time in the non-equilibrium evolution of a system of size N is $\text{var}(N) = \langle n(N)^2 \rangle - \langle n(N) \rangle^2$, where $n(N) = \sum_{i=1}^N n_i$. After some algebra, this can be written in terms of $\delta n_i \equiv n_i - c$ (as usual $c = \langle n_i \rangle$) as follows

$$\text{var}(N) = N \left\{ c(1-c) + \sum_{k \neq 0} \langle \delta n_i \delta n_{i+k} \rangle \right\}. \quad (\text{S10})$$

The anti-correlations due to the blockade effect are expected to decay at a finite distance for sufficiently large N . Indeed, starting from a very small N (within the blockade radius), $\sum_{k \neq 0} \langle \delta n_i \delta n_{i+k} \rangle$ is expected to become more and more negative as N grows, until N reaches beyond the Rydberg blockade radius, δn_i and δn_{i+k} for sufficiently large $|\mathbf{r}_i - \mathbf{r}_{i+k}|$ become independent ($\langle \delta n_i \delta n_{i+k} \rangle = 0$), and therefore $\sum_{k \neq 0} \langle \delta n_i \delta n_{i+k} \rangle$ saturates. In Figure 4 of the main text we show numerically obtained $\text{var}(N)/N$ as a function of N in a 1D lattice. The fact that the curves become flat for sufficiently large N is in agreement with the simple reasoning enunciated above. As expected, for small sizes a more complex dependence of the fluctuations on N is observed.

To understand the small N behaviour, we consider a simplified hard-objects model of the Rydberg blockade according to which every atom that is within the blockade radius R_B is in its ground state. For the sake of simplicity, we focus on the 1D case, although the same reasoning is expected to be relevant in lattices of higher dimensions. If $N \leq 2R_B$, then $\sum_{k \neq 0} \langle \delta n_i \delta n_{i+k} \rangle = (N-1)c(1-c)(-c)$. Here, c is the probability of having $n_i = 1$, i.e. an excitation at a generic site i , $(1-c)(-c)$ is the product of the fluctuations at i ($|\uparrow\rangle$) and $i+k$ ($|\downarrow\rangle$), and $N-1$ results from the

summation. We do not consider the case $n_i = 0$ because then $\langle \delta n_i \delta n_{i+k} \rangle = -c[c(1-c) + (1-c)(-c)] = 0$, where the term in square brackets includes the fluctuation for $|\uparrow\rangle$ and $|\downarrow\rangle$ states weighted by their probability of occurrence at $i+k$ (considering a ground state atom can be located at any distance from an excitation). When $N > 2R_B$, we obtain the aforementioned saturation $\sum_{k \neq 0} \langle \delta n_i \delta n_{i+k} \rangle = (2R_B - 1)c(1-c)(-c)$. Summarizing,

$$\text{var}(N) = \begin{cases} Nc(1-c)\{1 - (N-1)c\}, & N \leq 2R_B \\ Nc(1-c)\{1 - (2R_B - 1)c\}, & N > 2R_B. \end{cases} \quad (\text{S11})$$

Despite the simplicity of the approximation, Eq. (S11) is shown to be essentially valid in Figure 3 of the main text, highlighting its usefulness for studying the dynamical nature of the Rydberg blockade from macroscopic observations.

MEAN-FIELD APPROACH

The deposition dynamics is governed by the following equation

$$\partial_t |P(t)\rangle = \sum_k \Gamma_k [\sigma_+^k - (1 - n_k)] |P(t)\rangle. \quad (\text{S12})$$

Here, $|P(t)\rangle \equiv \sum_{\mathcal{C}} P(\mathcal{C}; t) |\mathcal{C}\rangle$, with $P(\mathcal{C}; t)$ the probability of configuration $|\mathcal{C}\rangle$ at time t . The operator σ_+^k creates an excitation at site k if the site is unexcited, and $n_k = |\uparrow\rangle_k \langle \uparrow|$ is the excitation number operator. The rate Γ_k is given in Eq. (1) in the main text. The average of the number operator corresponding to site j , $\langle n_j(t) \rangle = \langle -|n_j|P(t)\rangle$, with $|- \rangle \equiv \sum_{\mathcal{C}} |\mathcal{C}\rangle$, evolves in time according to $\partial_t \langle n_j(t) \rangle = \langle -|n_j \partial_t |P(t)\rangle = \sum_k \langle -|\Gamma_k n_j [\sigma_+^k - (1 - n_k)] |P(t)\rangle$.

In the mean-field approximation, $\partial_t \langle n_j(t) \rangle = \langle -|\Gamma_j (1 - n_j) |P(t)\rangle$, which, moreover, given the equivalence of all sites, $n_j(t) \rightarrow n(t)$, results in $\partial_t c(t) = \langle -|\Gamma(n(t)) (1 - n(t)) |P(t)\rangle$, where as usual $c(t) = \langle n(t) \rangle$. We can approximate this equation by replacing expectation values of products of operators by products of expectation values of operators: $\partial_t c(t) \approx \Gamma(c(t))(1 - c(t))$. The resulting mean-field equation for the time evolution of the density is

$$\partial_t c(t) = \frac{1 - c(t)}{1 + [F_\alpha R^\alpha c(t)]^2}. \quad (\text{S13})$$

Here, the geometric factor $F_\alpha \equiv \sum_k |\hat{\mathbf{r}}_k|^{-\alpha}$ converges for $\alpha > d$ and grows unboundedly for $\alpha \leq d$ as N is increased. It can be shown that the system asymptotically reaches the stationary solution $c_s = 1$.

For $\alpha > d$, we expect the existence of an initial stage, $c(t) \ll 1$, for which the denominator in Eq. (S13) is negligible, and there is an initial exponential growth $c(t) = 1 - \exp(-t)$. Physically, this corresponds to the creation of independent, distant excitations that eventually become the initial seed for the deposition process. In the case of $\alpha \leq d$, due to the unbounded growth of $F_\alpha \equiv \sum_k |\hat{\mathbf{r}}_k|^{-\alpha}$ with the system size, this regime is expected to be negligibly short for sufficiently large N . This is in agreement with the results reported in Figure 5 in the main text.

For a better understanding of the other regimes involved, we obtain the following implicit solution to Eq. (S13) by separation of variables: $t = -(1 + F_\alpha^2 R^{2\alpha}) \log(1 - c(t)) - (1/2) F_\alpha^2 R^{2\alpha} (2c(t) + c(t)^2)$. For long times, $c(t)$ is approximately 1 and the logarithmic term is dominant, which gives an exponential relaxation $c(t) \approx 1 - \exp(-t/(1 + F_\alpha^2 R^{2\alpha}))$. So the final stages of the mean field dynamics are ruled by exponential growth in all cases.

To study the intermediate time regime, for which $c(t)$ is still considerably smaller than 1, it is useful to expand the implicit solution in powers of $c(t)$: $t = c(t) + c(t)^2/2 + (1 + F_\alpha^2 R^{2\alpha}) [c(t)^3/3 + \mathcal{O}(c^4)]$. If $[F_\alpha R^\alpha c(t)]^2 \gg 1$, $c(t) \approx [3/(F_\alpha^2 R^{2\alpha})]^{1/3} t^{1/3}$. This is in agreement with the exponent $\gamma \approx 1/3$ observed for $\alpha \leq d$ in Figure 5 of the main text, as well as the fact that the prefactor of the power law increases as α becomes larger. For long-range interactions, $\alpha \leq d$, the dynamics is indeed effectively of the mean field type.

In conclusion, there are three distinct dynamical regimes qualitatively identical to those reported in Ref. [1]. For very short times, the creation of independent, distant excitations makes the concentration grow exponentially in time (for large N this is only observable if $\alpha > d$). For very long times, the system reaches exponentially the stationary state. Throughout most of the non-equilibrium evolution, the concentration grows algebraically according to the self-similar dynamics that has been thoroughly studied in the main text for $\alpha > d$, and following a mean-field dynamics with exponent $\gamma = 1/3$ in the long-range interacting case.

[1] I. Lesanovsky and J. P. Garrahan, Phys. Rev. Lett. **111**, 215305 (2013).